Supplementary Material for:

The evolution and distribution of recycled oceanic crust in the Earth's mantle: Insight from geodynamic models

Jun Yan[a], Maxim D. Ballmer[b, a, c], and Paul J. Tackley[a]

[a] Institute of Geophysics, ETH Zurich, Zurich, Switzerland

[b] Department of Earth Sciences, University College London, London, United Kingdom

[c] Earth-Life Science Institute, Tokyo Institute of Technology, Tokyo, Japan

Corresponding author: Jun Yan (jun.yan@erdw.ethz.ch)

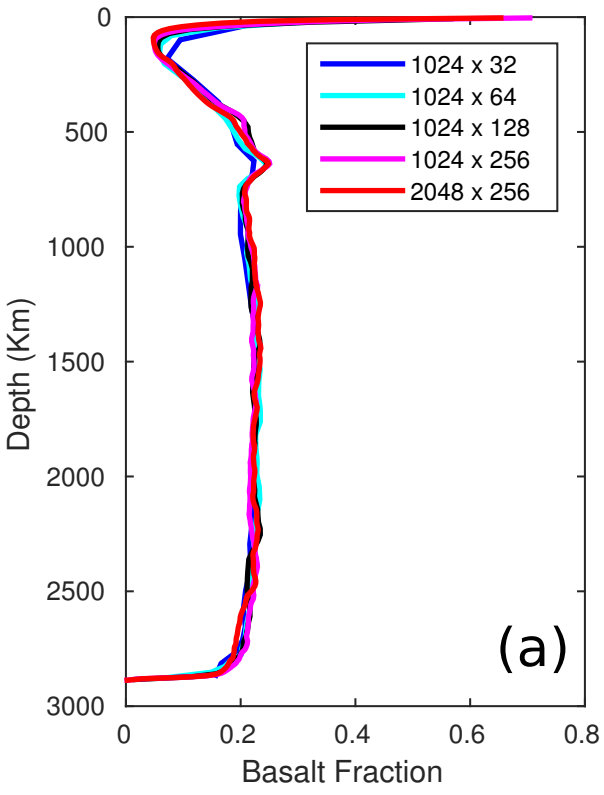
1024 x 32
1024 x 64
1024 x 128
1024 x 256
2048 x 256
Depth (Km)
Basalt Fraction
(a)

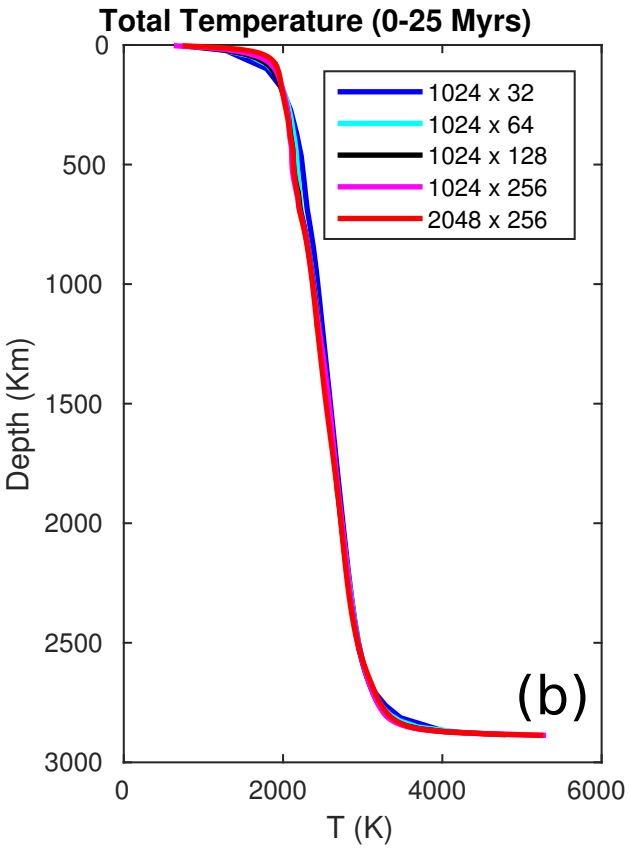
Total Temperature (0-25 Myrs)
1024 x 32
1024 x 64
1024 x 128
1024 x 256
2048 x 256
Depth (Km)
T (K)
(b)

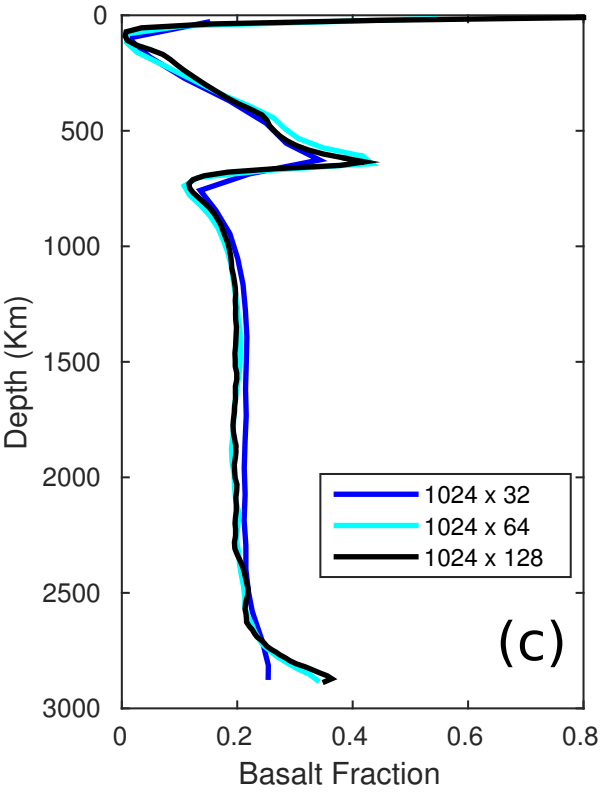
1024 x 32
1024 x 64
1024 x 128
Depth (Km)
Basalt Fraction
(c)

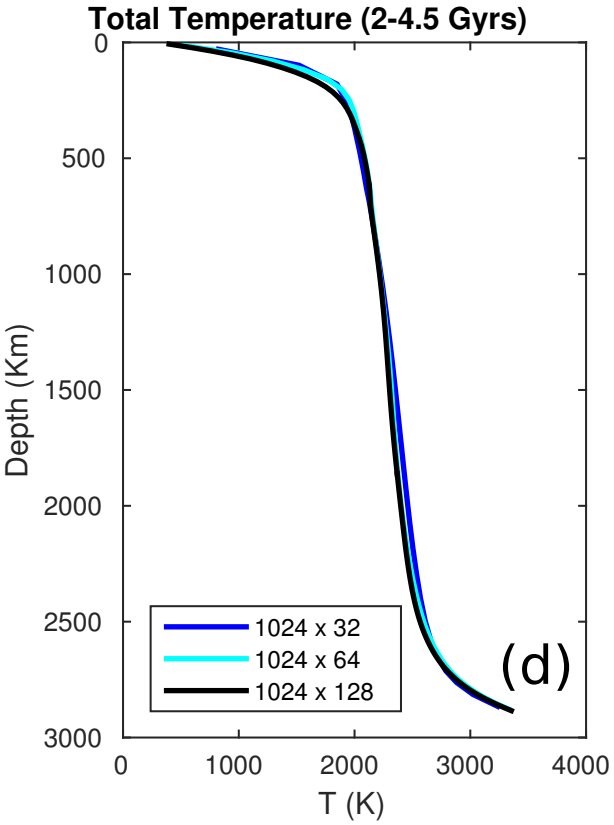
Total Temperature (2-4.5 Gyrs)
1024 x 32
1024 x 64
1024 x 128
Depth (Km)
T (K)
(d)

Fig. S1. Resolution test for cases with different resolution, but otherwise the same parameters as the reference case. A local grid refinement by up to 2 times near the surface and CMB (i.e., ~10 km radial grid spacing) is considered for all cases. Black line is the reference case with a resolution of 1024 × 128 cells. Radial average profiles of basalt fraction (a) and total temperature (b) from 0 to 25 Myr. Radial average profiles of basalt fraction (c) and total temperature (d) from 2 to 4.5 Gyr. Cases as labeled (The first and second numbers refer to the number of cells in the horizontal and radial directions, respectively). Note that two cases did not run much longer than 25 Myr due to computational limitations. We demonstrate that four cases (1024 × 64, 1024 × 128, 1024 × 256, and 2048 × 256) have very similar basalt-fraction and temperature profiles, hence confirming that the resolution used in our study is sufficient.

Table S1. Physical Parameters for Multicomponent Phase Changes. *i* and *j* are the indices for each relevant phase change.

#	Depth (*km*)	Temperature (*K*)	$\Delta\rho_{ph}\,(kgm^{-3})$	$\Gamma_{ph}\,(MPa/K)$	Width (*km*)
Olivine-Spinel-Perovskite-Postperovskite (system *i*=1)					
j=1	410	1600	280	2.1	29
j=2	660	1900	400	-1.8	29
j=3	2740	2650	62	7.2	29
Pyroxene-Garnet-Perovskite-Postperovskite (system *i*=2)					
j=1	60	0	350	0	29
j=2	300	1600	150	1.0	75
j=3	720	1900	500	0.7	75
j=4	2596	2560	62	7.2	29

Table S2. Physical parameters of mantle model. Reference viscosity is defined along the reference adiabat with T_a = 1600 K. Note that (*) denotes free parameter in our models, where $1.29\times10^{20} \leq \eta_0 \leq 1.29\times10^{22}$, $0.005 \leq \mu \leq 0.08$, $0.125 \leq \lambda_{410} \leq 8$, $7.5 \leq \lambda_{660} \leq 120$ and $0.02 \leq X_{BS} \leq 0.35$; all other parameters are fixed. Dimensional values listed above are for the reference model.

Notation	Parameter	Dimensional Value
η_0	Reference viscosity*	1.29×10^{21} $Pa\ s$
λ_{410}	Viscosity jump at 410 km*	1
λ_{660}	Viscosity jump at 660 km*	30
X_{BS}	Initial basalt fraction*	0.2
μ	Friction coefficient*	0.02
C	Cohesion coefficient at surface	4.6 MPa
D	Thickness of the mantle	2890 km
E	Activation energy	2.87×10^{5} $Jmol^{-1}$
V	Activation volume	2.49×10^{-6} m^3mol^{-1}
ρ_0	Reference (surface) density	3300 kgm^{-3}
g	Gravity	9.8 $m\ s^{-2}$
α_0	Reference (surface) thermal expansivity	5×10^{-5} K^{-1}
k_0	Reference (surface) thermal conductivity	3 $Wm^{-1}\ K^{-1}$
κ_0	Reference (surface) thermal diffusivity	7.58×10^{-7} m^2s^{-1}
Di	Surface dissipation number	1.3
γ	Reference (surface) Gruneisen parameter	1.3
T_a	Reference adiabat	1600 K
ΔT_{sa}	Temperature scale	2500 K

T_s	Surface temperature	300 K
H_r	Initial internal heating rate	1.58×10^{-11} Wkg^{-1}
L_h	Latent heat of fusion	6.0×10^{5} Jkg^{-1}
τ	Half life of internal heating	2.24 Gyr

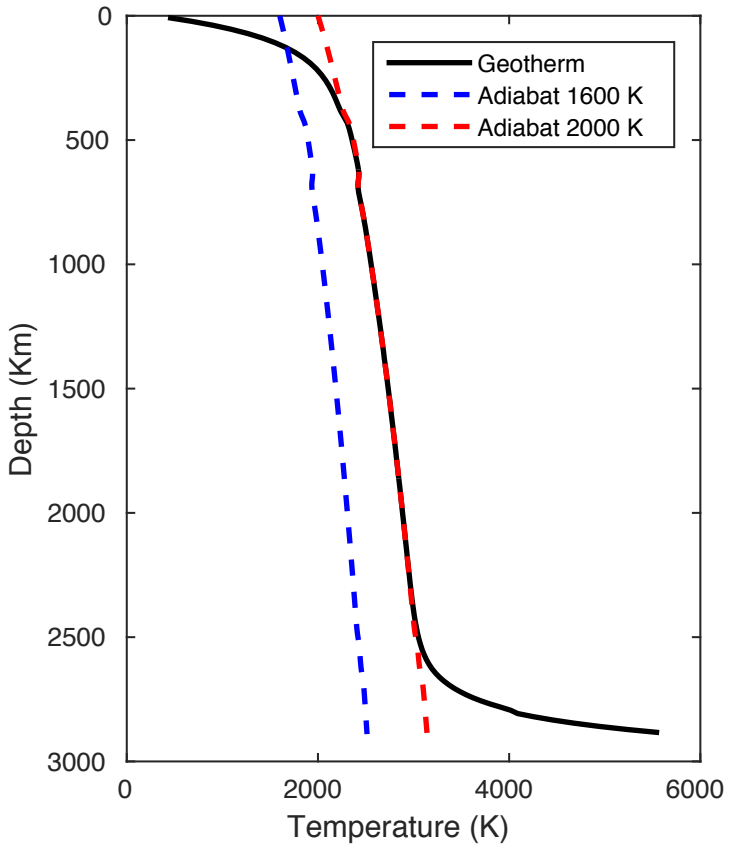

Fig. S2. Initial geotherm (i.e. real temperature profile) for all cases. Note that the initial geotherm is set to the 2000 K adiabat (red dashed line) across most of the mantle. In turn, physical properties (e.g., the density) are calculated along the 1600 K adiabat (blue dashed line) for all cases.

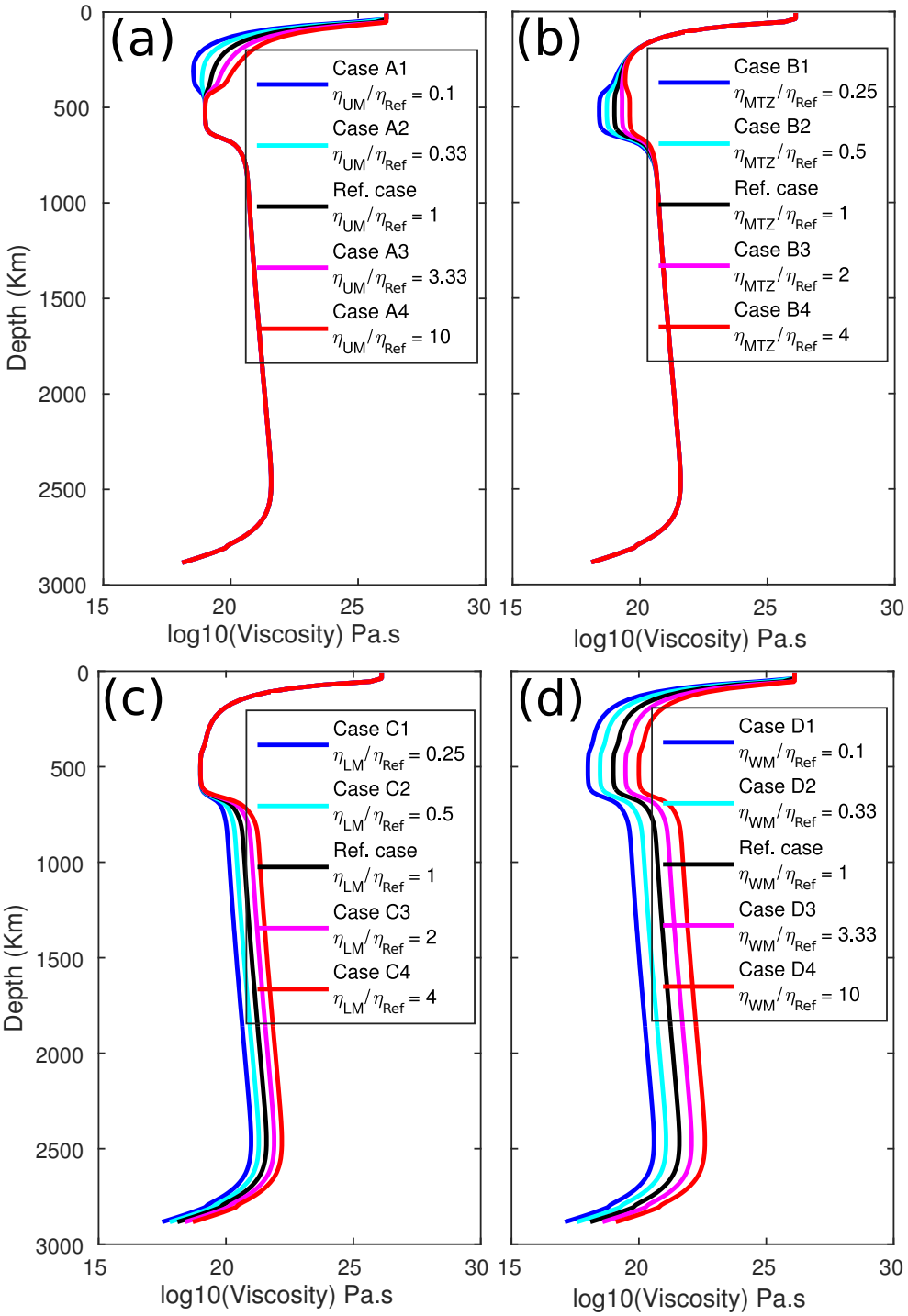

Fig. S3. Reference radial viscosity profiles for all cases in groups A-D as labeled. η_{UM}, η_{MTZ}, η_{LM} and η_{WM} denote uppermost-mantle viscosity, MTZ viscosity, lower-mantle viscosity, and

whole-mantle viscosity, respectively. Correspondingly, η_{Ref} denotes the viscosity of the reference case.

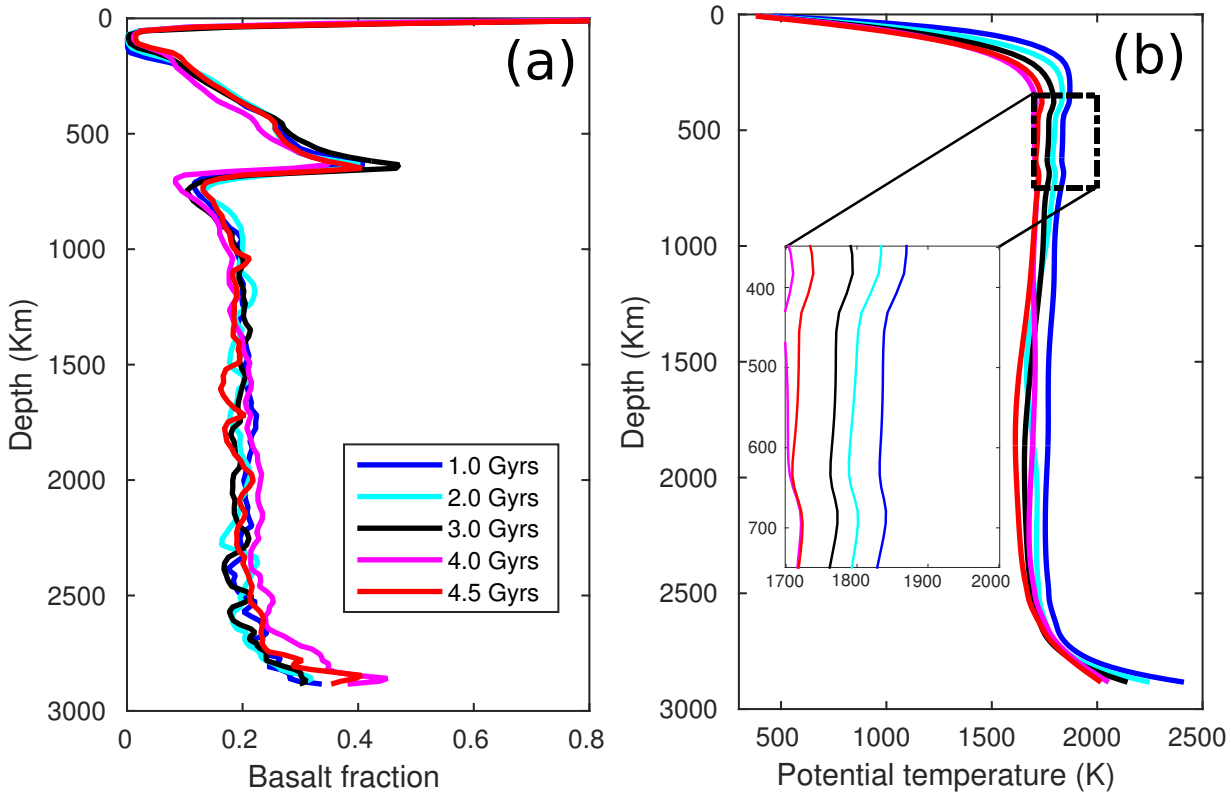

Fig. S4. Radial average profiles of (a) X_{BS} (compositional index) and (b) potential temperature for a test case with a low initial internal heating rate ($H_r = 3.4\times10^{-12}\ Wkg^{-1}$, other parameters are the same as those in the reference case) at different model times (from 1.0 to 4.5 Gyr as labeled). Note that the predicted radial average profiles of X_{BS} are very similar to that of reference case, but that predicted potential temperature is more realistic (see Fig. 3a-b in the text for comparison). H_r in this test case is lower than estimated for the bulk Earth's mantle (Lyubetskaya & Korenaga, J2007). However, this test case may mimic a situation, in which a

significant fractions of internal heat sources are stored near the CMB, e.g., due to partitioning of incompatible heat-producing elements into thermochemical piles. This interpretation is confirmed by Lourenço et al. (2018), see their Figure 1a-c.

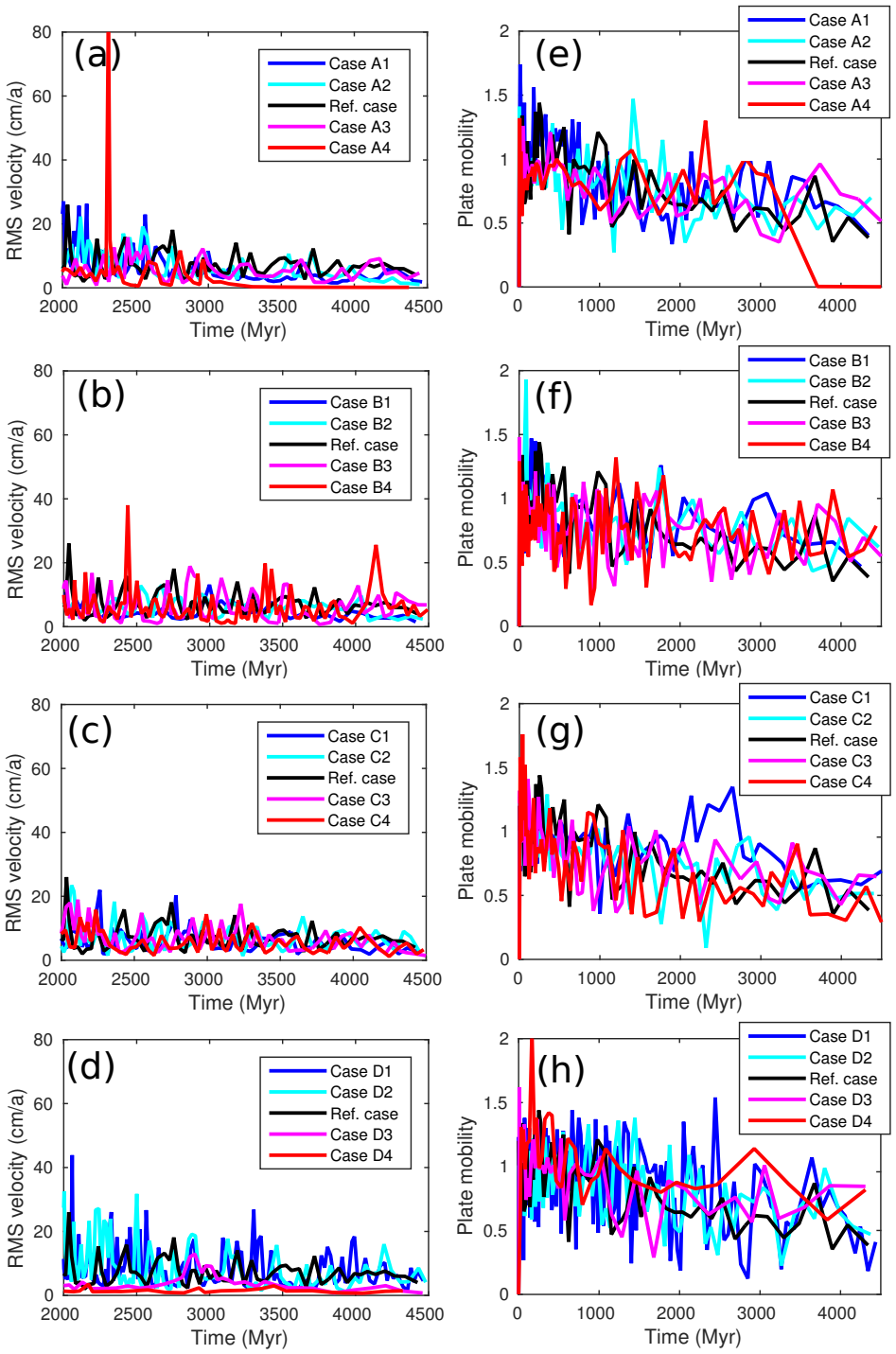

Fig. S5. Properties used to quantify Earth-like plate tectonic behavior. Left row: root-mean-square velocity of plates at the surface; right row: plate mobility as defined in Tackley (2000). Cases as labeled.

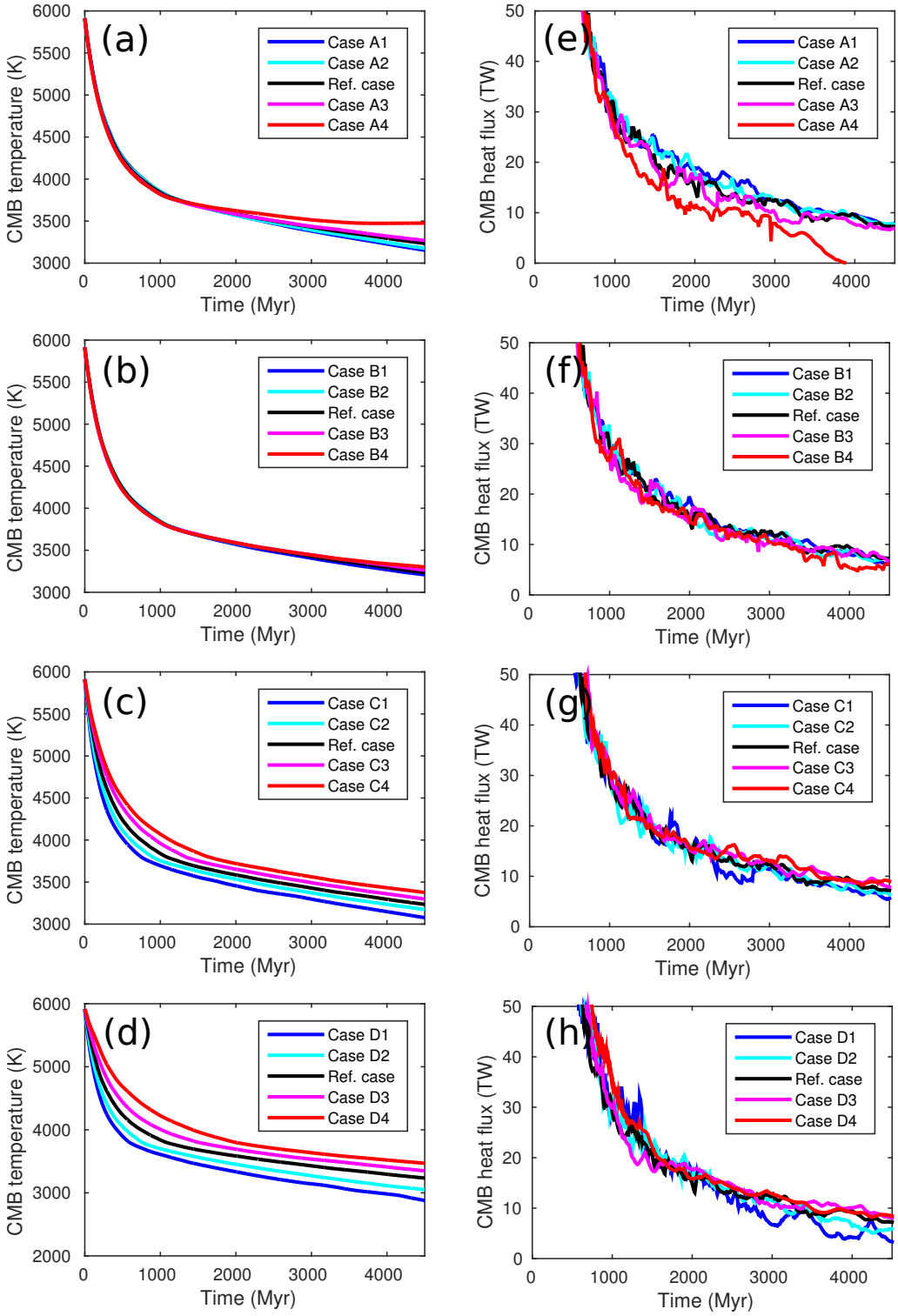

Fig. S6. Thermal evolution of the subset of models with variable viscosity profile. Left row: core-mantle boundary (CMB) temperature; right row: CMB heat flux. Cases as labeled.

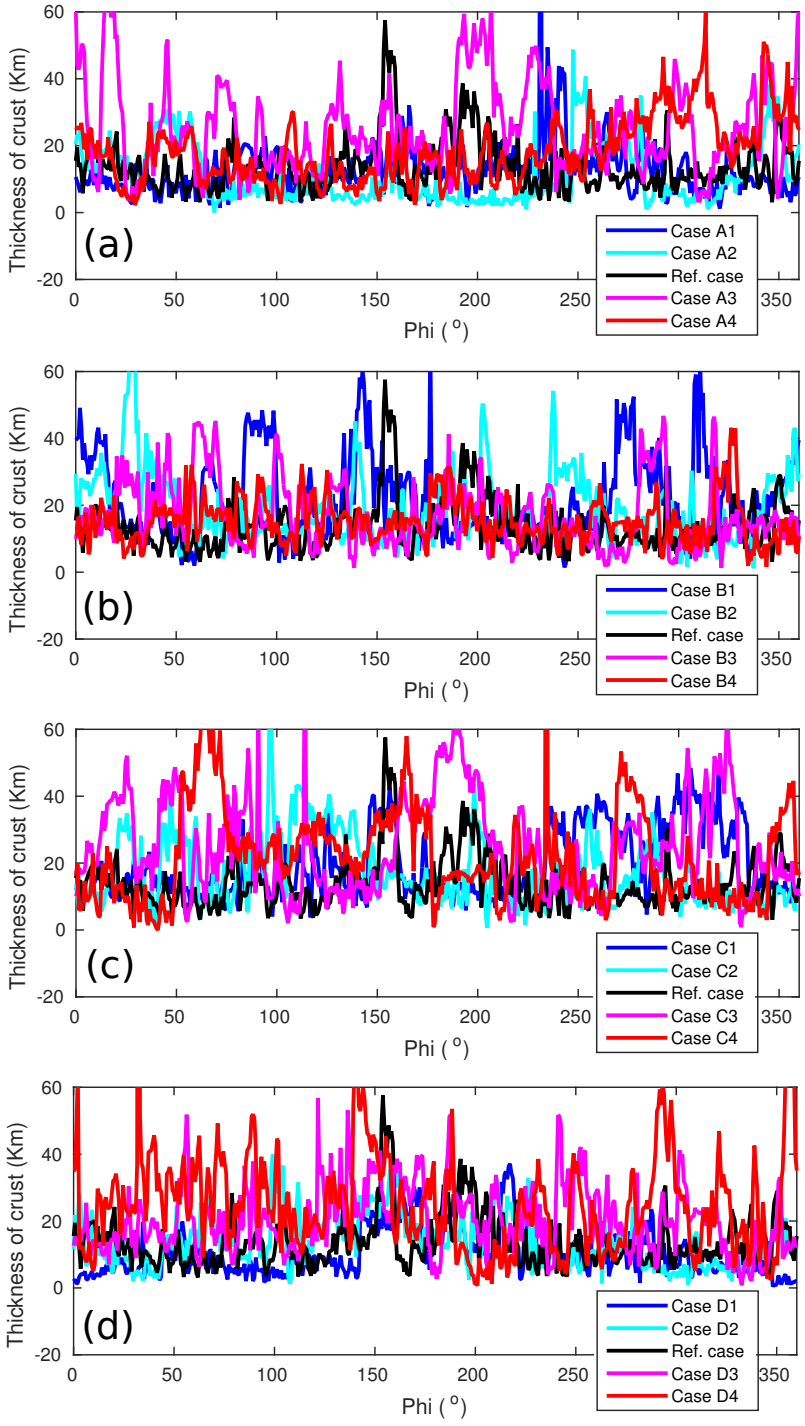

91

92 **Fig. S7**. Predicted crustal thickness along the surface at time 4.5 Gyr for a subset of cases

93 modeled. Phi is the longitude of the spherical-annulus model. Note that crustal thickness for the

94 reference case is < 15 km for much of the surface. Cases as labeled.

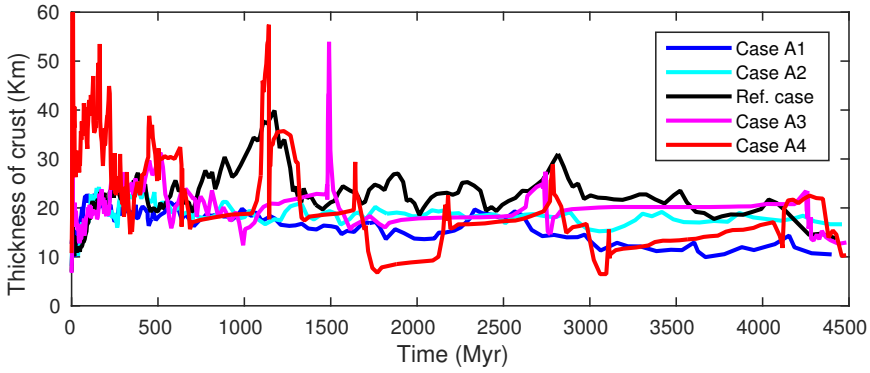
Thickness of crust (Km)
Time (Myr)
Case A1
Case A2
Ref. case
Case A3
Case A4

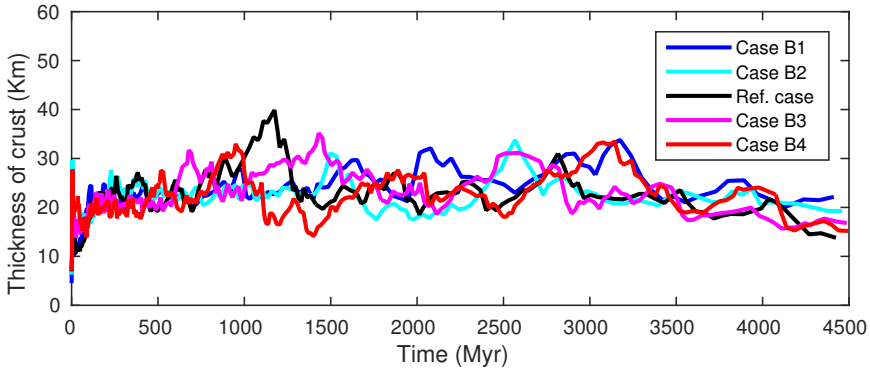
Thickness of crust (Km)
Time (Myr)
Case B1
Case B2
Ref. case
Case B3
Case B4

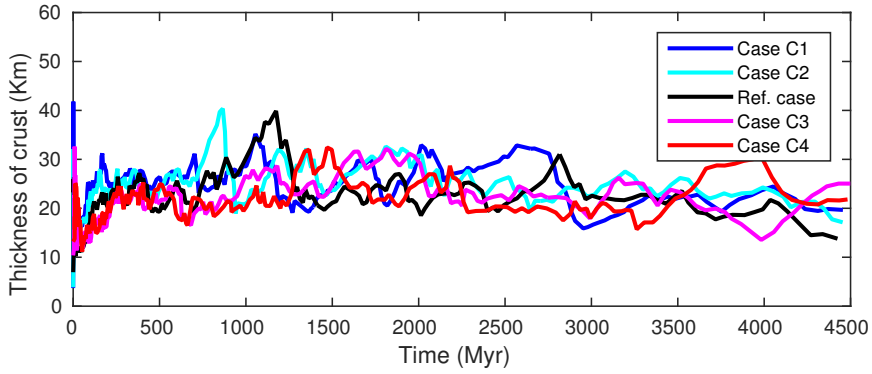
Thickness of crust (Km)
Time (Myr)
Case C1
Case C2
Ref. case
Case C3
Case C4

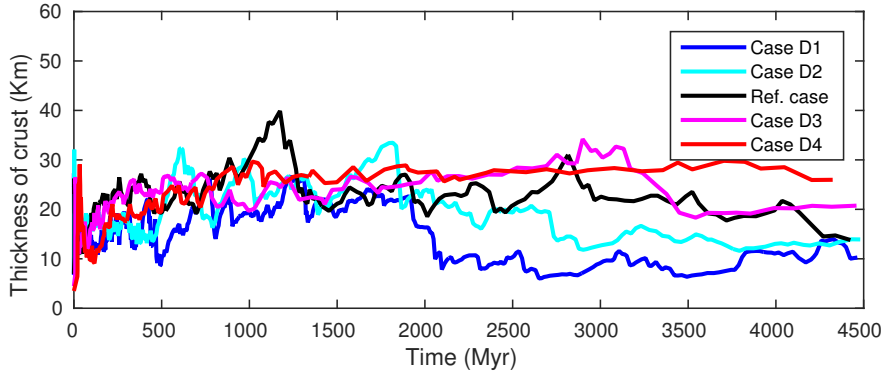
Thickness of crust (Km)
Time (Myr)
Case D1
Case D2
Ref. case
Case D3
Case D4

Fig. S8. Predicted crustal thickness (averaged along the surface) as a function of model time. Crustal thicknesses are slightly higher than those on Earth. Note however that crustal thicknesses in any given snapshot vary substantially (e.g. in regions of convergence) along the surface, and are smaller than the average for most regions (Fig. S6). Cases as labeled.

Movie S1: evolution of composition and temperature for the reference case

Movie S2: evolution of composition and temperature for case C1

Movie S3: evolution of composition and temperature for case C4

Movie S4: evolution of composition and temperature for case D1

References

Lourenço, D. L., Rozel, A. B., Gerya, T., & Tackley, P. J. (2018). Efficient cooling of rocky planets by intrusive magmatism. Nature Geoscience, 11(5), 322.

Lyubetskaya, T., & Korenaga, J. (2007). Chemical composition of Earth's primitive mantle and its variance: 2. Implications for global geodynamics. Journal of Geophysical Research: Solid Earth, 112(B3).

Tackley, P. J. (2000). Self-consistent generation of tectonic plates in time-dependent, three-dimensional mantle convection simulations. Geochemistry, Geophysics, Geosystems, 1(8).